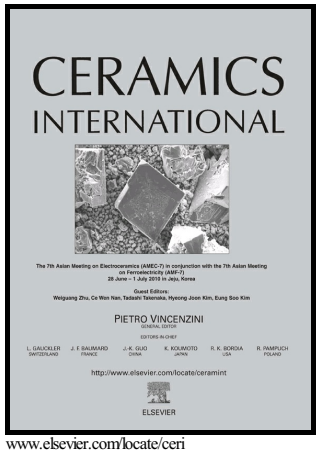

www.elsevier.com/locate/ceri

Reinforcing effects of SiC whiskers and carbon nanoparticles in spark plasma sintered ZrB_2 matrix composites

Yashar Azizian-Kalandaragh, Abbas Sabahi Namini, Zohre Ahmadi, Mehdi Shahedi Asl

PII: S0272-8842(18)32000-5
DOI: https://doi.org/10.1016/j.ceramint.2018.07.258
Reference: CERI18980

To appear in: *Ceramics International*

Received date: 9 July 2018
Revised date: 27 July 2018
Accepted date: 27 July 2018

Cite this article as: Yashar Azizian-Kalandaragh, Abbas Sabahi Namini, Zohre Ahmadi and Mehdi Shahedi Asl, Reinforcing effects of SiC whiskers and carbon nanoparticles in spark plasma sintered ZrB_2 matrix composites, *Ceramics International,* https://doi.org/10.1016/j.ceramint.2018.07.258

Reinforcing effects of SiC whiskers and carbon nanoparticles in spark plasma sintered ZrB_2 matrix composites

Yashar Azizian-Kalandaragh[a,b], Abbas Sabahi Namini[b,c], Zohre Ahmadi[d], Mehdi Shahedi Asl[e*]

[a]Department of Physics, University of Mohaghegh Ardabili, P.O. Box.179, Ardabil, Iran

[b]Department of Engineering Sciences, Sabalan University of Advanced Technologies(SUAT), Namin, Iran

[c]Department of Advanced Technologies, University of Mohaghegh Ardabili, Namin, Iran

[d]Young Researchers and Elite Club, Miyaneh Branch, Islamic Azad University, Miyaneh, Iran

[e]Department of Mechanical Engineering, University of Mohaghegh Ardabili, Ardabil, Iran

[*]Corresponding author: M. Shahedi Asl (shahedi@uma.ac.ir)

Abstract

ZrB_2-based ceramics, reinforced with 25 vol% SiC whiskers (SiC_w) as well as 0, 2.5, 5 and 7.5 wt% carbon nanoparticles (C_{np}), were prepared by spark plasma sintering (SPS) at 1900 ºC under 40 MPa for 7 min in a vacuum environment. The influences of C_{np} content on densification behavior, microstructure evolution, hardness and fracture toughness of ZrB_2–SiC_w ceramics were investigated. Compared to the carbon-free sample, the grain growth of ZrB_2 matrix was moderately decreased (~20%) after the addition of C_{np}. The in-situ formation of B_4C and ZrC phases was attributed to the elimination of surface oxide impurities through their chemical reactions with the C_{np} additive. All composite samples approached their theoretical densities. A hardness of 21.9 GPa was obtained for ZrB_2–SiC_w sample, but the hardness values linearly decreased by the addition of soft carbon additives and reached 14.6 GPa for the composite doped with 7.5 wt% C_{np}. The fracture toughness showed another trend and increased from 4.7 MPa $m^{½}$ for the carbon-free sample to 7.1 MPa $m^{½}$ for 5 wt% C_{np}-reinforced composite. The formation of new carbides and the presence of unreacted C_{np} resulted in toughness improvement. Various toughening mechanisms such as crack branching, bridging, and deflection were detected and discussed.

Keywords

ZrB_2; SiC whisker; carbon nanoparticle; spark plasma sintering; characterization

1. Introduction

Owing to its interesting physico-thermo-mechanical properties such as low density, high melting point, chemical inertness, high hardness and excellent electrical and thermal conductivity, ZrB_2 has increasingly attracted researchers' attention [1]–[5]. The densification of monolithic ZrB_2 ceramics requires ultrahigh sintering temperatures (>2000 ^{o}C) and externally applied pressures. Many different kinds of additives such as carbides [6]–[12], disilicides [13], [14], nitrides [15]–[18], metals [19], [20] and carbonaceous materials [21]–[29] are used to enhance the sinterability and densification capability of diboride-based composites. The addition of SiC, as the most interesting reinforcement in ZrB_2-based composites, not only enhances the sintering properties but also improves the flexural strength of composite material due to the prevention of growth of ZrB_2 grains during the sintering process [30]–[35].

However, the inadequate fracture toughness of ZrB_2–SiC composites impedes their widespread application in severe conditions. Earlier publications have proved that employing secondary phases with high aspect ratio morphologies such as flake, fiber, and whisker provides a favorable strategy to increase the mechanical properties of brittle ceramic matrix composites [36]–[45]. The addition of SiC whisker resulted in a remarkable increase in fracture toughness and flexural strength of ZrB_2 [41], [46]–[48]. SiC whisker can be pulled out or fractured during the crack propagation or activate several toughening mechanisms like crack bridging or deflection which leads to the fracture toughness enhancement [40], [49]–[52].

Anyway, SiC whisker may be degraded to SiC particulate at elevated sintering temperatures which is harmful to its strengthening effects [46], [53]. In such cases, the addition of the third phase seems to be necessary for the further improvement of fracture toughness. For example, the fracture toughness and flexural strength of ZrB_2-based ceramics were improved due to the synergistic addition of SiC whiskers and graphene nano-sheets [54]. In addition, the fracture toughness and thermal shock resistance of ZrB_2-based ceramics were remarkably improved by the simultaneous addition of SiC whiskers and graphite flakes whereas the flexural strength was slightly decreased [55]. Enhancement

of fracture toughness in carbon-doped ZrB_2–SiC ceramics was attributed to the presence of weak carbon interfaces at the grain boundaries after sintering process [56].

In this research work, the spark plasma sintering is employed to fabricate ZrB_2–25 vol% SiC_w composites using the different amounts of carbon nanoparticles (0, 2.5, 5 and 7.5 wt%) as extra dopant/reinforcement. The influences of C_{np} content on microstructural development as well as mechanical properties of ZrB_2–SiC_w ceramics are studied. To the best of our knowledge, this is the first attempt to employ SiC_w and C_{np}, simultaneously; to enhance the properties of spark plasma sintered ZrB_2-based ceramics.

2. Experimental procedure

2.1. Materials and process

Commercially available ZrB_2 powders, SiC whiskers (SiC_w) and plant-based carbon nanoparticles (C_{np}) were used as starting materials. Table 1 displays the technical characteristics of as-purchased materials. The powders were weighted, on account with the predetermined compositions itemized in Table 2, and dispersed separately in ethanol for 30-min ultrasonication. Succeeding that, the slurries of powder mixtures were ultrasonically mixed for an extra 30 min and dried on a hot plate stirrer. The prepared powders were milled in the agate mortar and then crossed through a 100-mesh sieve. After loading the mixtures into a graphite die (with inner 30-mm diameter), the spark plasma sintering was performed at a temperature of 1900 °C under a pressure of 40 MPa for a dwell time of 7 min.

Table 1. Technical characteristics of raw materials.

Materials	**Supplier**	**Purity (%)**	**Particle size**
ZrB_2	Xuzhou Hongwu (China)	99.9	D < 2 μm
SiC_w	Xuzhou Hongwu (China)	99.0	D < 1 μm, L < 20 μm
C	US Research Nanomaterials (USA)	99.0	10 nm < D < 30 nm

Table 2. Nomination and design of compositions of ZrB_2–SiC_w–C ceramics.

Code	**Composition**

ZSC_0	ZrB_2–25 vol% SiC_w
ZSC_1	ZrB_2–25 vol% SiC_w–2.5 wt% C
ZSC_2	ZrB_2–25 vol% SiC_w–5 wt% C
ZSC_3	ZrB_2–25 vol% SiC_w–7.5 wt% C

2.2. Characterization

The Archimedes principles were employed to estimate the bulk density of the sintered ceramics. The rule of mixtures was used to evaluate the theoretical density of composites assuming the true densities of 6.1, 3.2 and 0.5 g/cm^3 for the ZrB_2, SiC_w and C_{np}, respectively, based on the suppliers' datasheets. The ratio between the bulk and theoretical densities revealed the relative density value. The XRD test (PW1730, Philips) was used for phase analysis. The microstructural and elemental characterizations were carried out by FESEM (Mira3, Tescan) and EDS (DXP-X10P) analyses, respectively. The mean grain size of ZrB_2 matrix was calculated using an image analyzer (ImageJ software) through measuring the diameter of at least 120 grains. Thermodynamical assessments were conducted employing the HSC Chemistry package. Vickers indentation methodology was used to determine the hardness and fracture toughness by applying a load of 5 Kg for 15 s. A formula (Eq. 1) introduced by Anstis et al. [57] was employed for evaluation of indentation fracture toughness via the direct crack measurement technique.

$$K_{1C} = 0.016 \left(\frac{E}{H}\right)^{1/2} \left(\frac{L}{C^{3/2}}\right) \qquad (1)$$

where *E*, *H*, *L*, and *C* are the elastic modulus (calculated by the rule of mixtures), hardness (HV), load of Vickers indentation and half-length of the radial cracks (measured by an optical microscope), respectively.

3. Results and discussion

The characteristics of as-received ZrB_2 powders, the particle size of <2 μm and hexagonal crystalline structure, were reported in our previously published papers [20], [58], [59]. The size and morphology of SiC whiskers are presented in the FESEM image of Fig. 1 which

verifies the dominantly needle-like shapes for the raw SiC material. The TEM nanograph of Fig. 2 (provided by the supplier) shows the carbon nanoparticles with nano-sized diameters (<60 nm). The XRD analysis (not shown here) disclosed the hexagonal carbon as the dominant crystalline phase in the as-received C_{np} material.

Fig. 1. FESEM image of the morphology of as-purchased SiC whiskers.
Fig. 2. TEM image of the size and morphology of as-received carbon nanoparticles.

The relative density of as-sintered ZrB_2–SiC_w ceramics as a function of C_{np} content is shown in Fig. 3. A near fully dense ZrB_2–SiC_w composite (ZSC_0 sample) with a relative density of 99.9% was obtained by SPS at 1900 ºC for 7 min under 40 MPa without the addition of C_{np} as a dopant. By the addition of C_{np} (up to 5 wt%), slight enhancement in the relative density happened as the values of 100.1% and 100.2% were achieved for ZSC_1 and ZSC_2 samples, respectively. The extraordinary measurements of higher than 100% for the relative density of carbon-doped composites can be attributed to the in-situ formation of some heavier phases during the sintering. It should be noted that the density values of such in-situ formed phases are not inserted in the relative density estimations using the rule of mixtures. It seems that the addition of extra C_{np} (7.5 wt%) has a negative effect on the densification progress of ZSC_3 sample since a relative density of 99.8% was measured for this composite.

Fig. 3. Relative density of ZrB_2–SiC_w ceramics as a function of nano-carbon content.

Fig. 4 shows the XRD results of the as-sintered ZSC_3 sample which contains the highest amount of C_{np}. The main starting materials of ZrB_2 (as the matrix) and SiC (as the reinforcement) are detected as the dominant phases in this pattern. As an expected characteristic for the silicon carbide whiskers, the crystalline structure of the SiC phase is “cubic”, based on the XRD analysis. Two peaks of graphite are also detected; hence, it seems that the remained carbon nanoparticles with a hexagonal structure have morphologically transformed to the graphite with same crystalline lattice, maybe due to the externally applied pressure during the sintering process. The nano-scale graphitized C_{np} with flaky morphology is presented in Fig. 5, the FESEM nanograph of the fracture surface

of ZSC_2 composite. Moreover, the in-situ formation of new carbides (B_4C and ZrC) to a small amount is also confirmed by the XRD analysis.

Fig. 4. XRD pattern of the sintered ZSC_3 sample.
Fig. 5. FESEM nanograph of carbon (graphite) nano-flakes in the fracture surface of ZSC_3 sample.

The FESEM images of the polished surfaces of as-sintered ZrB_2–SiC_w ceramics, with various C_{np} additions, are displayed in Fig. 6. Fig. 6a shows a homogenous distribution of SiC grains in the ZrB_2 matrix. This micrograph verifies a complete densification and fully-progressed sintering in the ZSC_0 sample as the ZrB_2 and SiC particles have well connected together. No obvious porosity is seen in Fig. 6a and the relative density of 99.9% for this ceramic is in harmony with such microstructural observation. Although most of the SiC whiskers have lost their morphological features during the SPS process, some of them are remained in the final microstructure (marked by arrows in Fig. 6a). The presence of in-situ formed phases is clearly seen in the FESEM micrographs of C_{np}-doped ZrB_2–SiC_w composites (Fig. 6b-d). For example, a graphitized carbon/in-situ formed new carbides area is marked by an arrow in the microstructure of ZSC_1 ceramic presented in Fig. 6b. In addition, some negligible pores are detected in the FESEM micrograph of ZSC_3 ceramic (Fig. 6d) may be due to its relative density value of 99.8%. It appears that the extra addition of C_{np} (e.g. 7.5 wt%) in the ZrB_2–SiC_w ceramics resulted in the agglomeration of carbon-induced graphite nano-flakes which have not fully sintered to be able to remove the pores completely.

Fig. 6. FESEM images (backscattered electron mode) of the polished surfaces of carbon-doped ZrB_2–SiC_w ceramics: (a) ZSC_0, (b) ZSC_1, (c) ZSC_2 and (d) ZSC_3.

The average grain size of ZrB_2 matrix in the sintered samples, as a function of C_{np} content, is reported in Fig. 7. In comparison with the starting particle of 2-µm for ZrB_2, no fanatic grain growth was happened during the SPS process, even in the carbon-free ZSC_0 sample with a mean ZrB_2 grain size of 5.2 µm. The introduction of C_{np}, regardless of its content, led to a better grain growth inhibition in ZSC_1, ZSC_2, and ZSC_3 composites. The finest microstructure belongs to the ZSC_2 sample with an average ZrB_2 grain size of 4.1 µm.

Besides the short dwelling time of 7-min for the SPS process, the beneficial effects of SiC_w and C_{np} additives on fabricating a fine-grained microstructure are revealed by such observations.

Fig. 7. Average ZrB_2 grain size in the as-sintered ZrB_2–SiC_w ceramics as a function of nano-carbon content.

The Gibbs free energy variations of the chemical reactions of SiC_w and C_{np} additives with the oxide layers in the ZrB_2–SiC_w–C_{np} system, leading to the conversion of harmful oxides to the useful ZrB_2 and SiC ultrafine grains, are presented in Fig. 8. The SiC is ordinarily a non-reactive secondary phase in ZrB_2-based systems; however, a chemical reaction between the SiC_w and the surface oxide layers of ZrO_2 and B_2O_3 (Eq. 2) is thermodynamically favorable at >1760 °C (Fig. 8). Hence, the ultrafine ZrB_2 particles with higher sinterability can be formed. The gaseous byproducts of SiO and CO can be removed during the SPS process due to the applied pressure on the die and vacuum condition of the sintering furnace.

$$5SiC_w + 2ZrO_2 + 2B_2O_3 = 2ZrB_2 + 5SiO\ (g) + 5CO\ (g) \qquad (2)$$

Similar to the reductive role of SiC_w (Eq. 2), the C_{np} can also eliminate the surface oxide impurities of ZrB_2 powders in accord with the reaction of Eq. 3. Thermodynamically, the C_{np} is more effective reductant than the SiC_w, because Eq. 3 occurs at a remarkably lower temperature (>1515 ºC) than that required for Eq. 2.

$$5C_{np} + ZrO_2 + B_2O_3 = ZrB_2 + 5CO\ (g) \qquad (3)$$

The C_{np} not only can remove the oxide layers of ZrB_2 particles, but also the surface impurities of SiC_w (particularly SiO_2) based on the chemical reaction of Eq. 4. This equation is also favorable at >1515 ºC.

$$3C_{np} + SiO_2 = SiC + 2CO\ (g) \qquad (4)$$

Fig. 8. Gibbs free energy of elimination reactions of oxide layers leading to the formation of ultrafine ZrB_2 and SiC (extracted by HSC Chemistry package).

Fig. 9 shows the variations of Gibbs free energy for the reductive reactions of C_{np} with ZrO_2 and B_2O_3 impurities leading to the in-situ formation of B_4C and ZrC. Based on the thermodynamics, the chemical reactions of Eq. 5 (the formation of ZrC) and Eq. 6 (the formation of B_4C) are favorable at the temperatures higher than 1670 ºC and 1570 ºC, respectively. The formation of B_4C and ZrC compounds in the spark plasma sintered C_{np}-doped ZrB_2–SiC_w composites is previously proved by the XRD analyses (Fig. 4).

$$3C_{np} + ZrO_2 = ZrC + 2CO\ (g) \qquad (5)$$

$$7C_{np} + 2B_2O_3 = B_4C + 6CO\ (g) \qquad (6)$$

Fig. 9. Gibbs free energy of elimination reactions of oxide layers leading to the in-situ formation of ZrC and B_4C (extracted by HSC Chemistry package).

Fig. 10 presents the hardness of as-sintered ZrB_2–SiC_w ceramics as a function of C_{np} content. A value of 21.9 GPa was measured for the ZSC_0 sample as the highest hardness value in the current work. As a comparison, a hardness of 19.5 GPa was reported by our research group [60] for the SiC particulate reinforced ZrB_2-based ceramic with similar processing conditions, composition, and relative density. Therefore, it seems that the SiC whiskers can resist in a superior way than the SiC particulates against the plastic deformation during the hardness measurement test. However, as it can be obviously observed in Fig. 10, the hardness of the samples drops with increasing the C_{np} content. The ZSC_3 sample with a hardness of 14.6 GPa is the softest sample in this research work. The presence of unreacted C_{np} in the sintered microstructures, even in the form of graphite which is intrinsically softer than ZrB_2 and SiC_w, led to the sharp decrease in the hardness values of the C_{np}-doped composites.

Fig. 10. Hardness (HV5) of ZrB_2–SiC_w ceramics as a function of nano-carbon content.

Fig. 11 presents the fracture toughness of ZrB_2–SiC_w samples as a function of C_{np} content. A fracture toughness of 4.7 MPa $m^{½}$ is estimated for the ZSC_0 sample which is ~10% higher than the value reported for a similar composite reinforced with the SiC particulates (4.3 MPa $m^{½}$) [60]. The fracture toughness improves to 7.1 MPa $m^{½}$ with increasing the C_{np} content up to 5 wt%. Such a significant increase in the fracture toughness of ZSC_2 sample is related to the synergistic toughening effects of SiC whiskers and carbon nanoparticles. Having the finest microstructure, the presence of SiC_w and graphite as reinforcement phases in the sintered microstructure and the in-situ formation of B_4C and ZrC compounds during the SPS process are the main boosters of fracture toughness of ZSC_2 sample. However, the addition of 7.5 wt% C_{np} does not have a meaningful enhancement in the fracture toughness value since a fracture toughness of 7.2 MPa $m^{½}$ is measured for the ZSC_3 sample.

Fig. 11. Indentation fracture toughness of ZrB_2–SiC_w ceramics as a function of nano-carbon content.

Fig. 12 shows the FESEM images of crack paths induced by Vickers indenter in the polished surfaces of ZSC_1 sample. Several crack deflections, as an important toughening mechanism in ceramic matrix composites, are seen in Fig. 12a. Such deflections generally occur due to the interaction of propagating cracks with the secondary phases in the composites, namely, the SiC_w, graphitized C_{np}, ZrC or B_4C in this study. More crack deflections with greater deviation angles result in improved fracture toughness because further energy is absorbed during the propagation of the indentation-induced crack. Crack branching, another toughening mechanism, is also seen in Fig. 12a, as a result of the interaction of the main crack with the secondary phases, especially with the softer ones such as C_{np}/graphite. Fig. 12b presents the activation of another consequential toughening mechanism, crack bridging, due to the presence of various reinforcements in the final sintered microstructure. Beside the mentioned toughening mechanisms, break of a large SiC grain is seen in Fig. 12c which leads to the diminution of the propagating energy of the main crack.

Fig. 12. FESEM micrographs of several indentation-induced crack paths in the polished surface of ZSC_1 composite.

The high-magnification FESEM image of a crack path in the polished surface of ZSC_2 sample is shown in Fig. 13a. The related EDS maps, showing the elemental distribution in different phases of this composite, are also presented in Fig. 13b-f. The activation of various toughening mechanisms such as crack bridging and deflection is clearly seen in the FESEM image (Fig. 13a). The improved fracture toughness value of ZSC_2 ceramic may be related to the presence/in-situ formation of ultrafine reinforcements of SiC_w and graphitized C_{np}, with high aspect ratios, in its final microstructure. The interactions between the indentation-induced propagating cracks and the composite microstructure are generally controlled by the intensity of residual stresses. The mismatch between the thermal and mechanical properties (for example, the coefficients of thermal expansions and elastic moduli) of the matrix and the secondary phases lead to the formation of such residual stresses.

Fig. 13. (a) High-magnification FESEM image (Secondary electron mode) of an indentation-induced crack path in the polished surface of ZSC_2 composite and (b-f) corresponding EDS elemental maps.

4. Conclusions

SiC whisker (25 vol%) reinforced ZrB_2-based composites, doped with 0, 2.5, 5 and 7.5 wt% carbon nanoparticles, were manufactured by spark plasma sintering route at the temperature of 1900 ºC. All ceramic samples reached >99.8% of their theoretical densities but the introduction of carbon additive, regardless of its content, resulted in grain growth inhibition. The harmful oxide impurities were eliminated via reacting with the carbon and converted to useful ZrC and B_4C compounds. With increasing the nano-carbon content in ZrB_2–SiC_w composites, the fracture toughness remarkably increased but the hardness critically deceased. The presence of unreacted carbon nanoparticles and the in-situ formation of interfacial carbides led to the actuation of several toughening mechanisms like crack deflection, branching and bridging in ZrB_2–SiC_w ceramics.

References

[1] M. Jaberi Zamharir, M. Shahedi Asl, M. Ghassemi Kakroudi, N. Pourmohammadie Vafa, and M. Jaberi Zamharir, "Significance of hot pressing parameters and reinforcement size on sinterability and mechanical properties of ZrB_2–25vol% SiC UHTCs," *Ceram. Int.*, vol. 41, no. 8, pp. 9628–9636, 2015.

[2] M. Shahedi Asl, M. Ghassemi Kakroudi, M. Rezvani, and F. Golestani-Fard, "Significance of hot pressing parameters on the microstructure and densification behavior of zirconium diboride," *Int. J. Refract. Met. Hard Mater.*, vol. 50, pp. 140–145, 2015.

[3] M. Jaberi Zamharir, M. Shahedi Asl, N. Pourmohammadie Vafa, and M. Ghassemi Kakroudi, "Significance of hot pressing parameters and reinforcement size on densification behavior of ZrB_2–25vol% SiC UHTCs," *Ceram. Int.*, vol. 41, no. 5, pp. 6439–6447, 2015.

[4] B. Nayebi, M. Shahedi Asl, M. Ghassemi Kakroudi, I. Farahbakhsh, and M. Shokouhimehr, "Interfacial phenomena and formation of nano-particles in porous ZrB_2–40 vol% B_4C UHTC," *Ceram. Int.*, vol. 42, no. 15, pp. 17009–17015, 2016.

[5] M. Shahedi Asl, M. Ghassemi Kakroudi, B. Nayebi, and H. Nasiri, "Taguchi analysis on the effect of hot pressing parameters on density and hardness of zirconium diboride," *Int. J. Refract. Met. Hard Mater.*, vol. 50, pp. 313–320, 2015.

[6] M. Shahedi Asl, Z. Ahmadi, S. Parvizi, Z. Balak, and I. Farahbakhsh, "Contribution of SiC particle size and spark plasma sintering conditions on grain growth and hardness of TiB_2 composites," *Ceram. Int.*, vol. 43, no. 16, pp. 13924–13931, 2017.

[7] Z. Ahmadi, B. Nayebi, M. Shahedi Asl, I. Farahbakhsh, and Z. Balak, "Densification improvement of spark plasma sintered TiB_2-based composites with micron-, submicron- and nano-sized SiC particulates," *Ceram. Int.*, vol. 44, no. 10, pp. 11431–11437, 2018.

[8] B. Nayebi, M. Shahedi Asl, M. Ghassemi Kakroudi, and M. Shokouhimehr, "Temperature dependence of microstructure evolution during hot pressing of ZrB_2–30 vol.% SiC composites," *Int. J. Refract. Met. Hard Mater.*, vol. 54, pp. 7–13, 2016.

[9] A. Sabahi Namini, S. N. Seyed Gogani, M. Shahedi Asl, K. Farhadi, M. Ghassemi Kakroudi, and A. Mohammadzadeh, "Microstructural development and mechanical properties of hot pressed SiC reinforced TiB_2 based composite," *Int. J. Refract. Met. Hard Mater.*, vol. 51, pp. 169–179, 2015.

[10] M. Shahedi Asl, M. Ghassemi Kakroudi, and S. Noori, "Hardness and toughness of hot pressed ZrB_2–SiC composites consolidated under relatively low pressure," *J. Alloys Compd.*, vol. 619, pp. 481–487, 2015.

[11] M. Shahedi Asl and M. Ghassemi Kakroudi, "Fractographical assessment of densification mechanisms in hot pressed ZrB_2–SiC composites," *Ceram. Int.*, vol. 40, no. 9, pp. 15273–15281, 2014.

[12] M. Shahedi Asl, M. Ghassemi Kakroudi, and B. Nayebi, "A fractographical approach to the sintering process in porous ZrB_2–B_4C binary composites," *Ceram. Int.*, vol. 41, no. 1, pp. 379–387, 2015.

[13] S.-Q. Guo, Y. Kagawa, T. Nishimura, and H. Tanaka, "Pressureless sintering and physical properties of ZrB_2-based composites with $ZrSi_2$ additive," *Scr. Mater.*, vol. 58, no. 7, pp. 579–582, 2008.

[14] D. Sciti, M. Brach, and A. Bellosi, "Oxidation behavior of a pressureless sintered ZrB_2–$MoSi_2$ ceramic composite," *J. Mater. Res.*, vol. 20, no. 04, pp. 922–930, 2005.

[15] Z. Ahmadi, B. Nayebi, M. Shahedi Asl, and M. Ghassemi Kakroudi, "Fractographical characterization of hot pressed and pressureless sintered AlN-doped ZrB_2–SiC composites," *Mater. Charact.*, vol. 110, pp. 77–85, 2015.

[16] Z. Ahmadi, B. Nayebi, M. Shahedi Asl, M. Ghassemi Kakroudi, and I. Farahbakhsh, "Sintering behavior of ZrB_2–SiC composites doped with Si_3N_4: a fractographical approach," *Ceram. Int.*, vol. 43, no. 13, pp. 9699–9708, 2017.

[17] Z. Hamidzadeh Mahaseni, M. Dashti Germi, Z. Ahmadi, and M. Shahedi Asl, "Microstructural investigation of spark plasma sintered TiB_2 ceramics with Si_3N_4 addition," *Ceram. Int.*, vol. 44, no. 11, pp. 13367–13372, 2018.

[18] M. Shahedi Asl, B. Nayebi, Z. Ahmadi, P. Pirmohammadi, and M. Ghassemi Kakroudi, "Fractographical characterization of hot pressed and pressureless sintered SiAlON-doped ZrB_2–SiC

composites," *Mater. Charact.*, vol. 102, pp. 137–145, 2015.
[19] E. Ghasali and M. Shahedi Asl, "Microstructural development during spark plasma sintering of ZrB_2–SiC–Ti composite," *Ceram. Int.*, 2018, doi:10.1016/j.ceramint.2018.07.011.
[20] M. Shahedi Asl, B. Nayebi, Z. Ahmadi, S. Parvizi, and M. Shokouhimehr, "A novel ZrB_2–VB_2–ZrC composite fabricated by reactive spark plasma sintering," *Mater. Sci. Eng. A*, vol. 731, pp. 131–139, 2018.
[21] M. Shahedi Asl, F. Golmohammadi, M. Ghassemi Kakroudi, and M. Shokouhimehr, "Synergetic effects of SiC and C_{sf} in ZrB_2-based ceramic composites. Part I: densification behavior," *Ceram. Int.*, vol. 42, no. 3, pp. 4498–4506, 2016.
[22] M. Shahedi Asl, B. Nayebi, and M. Shokouhimehr, "TEM characterization of spark plasma sintered ZrB_2–SiC–graphene nanocomposite," *Ceram. Int.*, vol. 44, no. 13, pp. 15269–15273, 2018.
[23] M. Shahedi Asl, B. Nayebi, Z. Ahmadi, M. Jaberi Zamharir, and M. Shokouhimehr, "Effects of carbon additives on the properties of ZrB_2–based composites: a review," *Ceram. Int.*, vol. 44, no. 7, pp. 7334–7348, 2018.
[24] M. Shahedi Asl, "Microstructure, hardness and fracture toughness of spark plasma sintered ZrB_2–SiC–C_f composites," *Ceram. Int.*, vol. 43, no. 17, pp. 15047–15052, 2017.
[25] I. Farahbakhsh, Z. Ahmadi, and M. Shahedi Asl, "Densification, microstructure and mechanical properties of hot pressed ZrB_2–SiC ceramic doped with nano-sized carbon black," *Ceram. Int.*, vol. 43, no. 11, pp. 8411–8417, 2017.
[26] M. Shahedi Asl, M. Ghassemi Kakroudi, I. Farahbakhsh, B. Mazinani, and Z. Balak, "Synergetic effects of SiC and C_{sf} in ZrB_2-based ceramic composites. Part II: grain growth," *Ceram. Int.*, vol. 42, no. 16, pp. 18612–18619, 2016.
[27] M. Shahedi Asl, I. Farahbakhsh, and B. Nayebi, "Characteristics of multi-walled carbon nanotube toughened ZrB_2–SiC ceramic composite prepared by hot pressing," *Ceram. Int.*, vol. 42, no. 1, pp. 1950–1958, 2016.
[28] M. Shahedi Asl, M. Ghassemi Kakroudi, R. Abedi Kondolaji, and H. Nasiri, "Influence of graphite nano-flakes on densification and mechanical properties of hot-pressed ZrB_2–SiC composite," *Ceram. Int.*, vol. 41, no. 4, pp. 5843–5851, 2015.
[29] M. Shahedi Asl and M. Ghassemi Kakroudi, "Characterization of hot-pressed graphene reinforced ZrB_2–SiC composite," *Mater. Sci. Eng. A*, vol. 625, pp. 385–392, 2015.
[30] M. Shahedi Asl, M. Ghassemi Kakroudi, F. Golestani-Fard, and H. Nasiri, "A Taguchi approach to the influence of hot pressing parameters and SiC content on the sinterability of ZrB_2-based composites," *Int. J. Refract. Met. Hard Mater.*, vol. 51, pp. 81–90, 2015.
[31] M. Shahedi Asl, A. Sabahi Namini, and M. Ghassemi Kakroudi, "Influence of silicon carbide addition on the microstructural development of hot pressed zirconium and titanium diborides," *Ceram. Int.*, vol. 42, no. 4, pp. 5375–5381, 2016.
[32] Z. Balak, M. Azizieh, H. Kafashan, M. Shahedi Asl, and Z. Ahmadi, "Optimization of effective parameters on thermal shock resistance of ZrB_2-SiC-based composites prepared by SPS: using Taguchi design," *Mater. Chem. Phys.*, vol. 196, pp. 333–340, 2017.
[33] Z. Balak, M. Shahedi Asl, M. Azizieh, H. Kafashan, and R. Hayati, "Effect of different additives and open porosity on fracture toughness of ZrB_2–SiC-based composites prepared by SPS," *Ceram. Int.*, vol. 43, no. 2, pp. 2209–2220, 2017.
[34] N. Pourmohammadie Vafa, M. Shahedi Asl, M. Jaberi Zamharir, and M. Ghassemi Kakroudi, "Reactive hot pressing of ZrB_2-based composites with changes in ZrO_2/SiC ratio and sintering conditions. Part I: densification behavior," *Ceram. Int.*, vol. 41, no. 7, pp. 8388–8396, 2015.
[35] N. Pourmohammadie Vafa, B. Nayebi, M. Shahedi Asl, M. Jaberi Zamharir, and M. Ghassemi Kakroudi, "Reactive hot pressing of ZrB_2-based composites with changes in ZrO_2/SiC ratio and sintering conditions. Part II: Mechanical behavior," *Ceram. Int.*, vol. 42, no. 2, pp. 2724–2733, 2016.
[36] E. Ghasali, T. Ebadzadeh, M. Alizadeh, and M. Razavi, "Spark plasma sintering of WC-based cermets/titanium and vanadium added composites: a comparative study on the microstructure and mechanical properties," *Ceram. Int.*, vol. 44, no. 9, pp. 10646–10656, 2018.
[37] S. I. Golestaneh, G. Karimi, A. Babapoor, and F. Torabi, "Thermal performance of co-electrospun fatty acid nanofiber composites in the presence of nanoparticles," *Appl. Energy*, vol. 212, pp. 552–564, 2018.

[38] E. Ghasali, K. Shirvanimoghaddam, M. Alizadeh, and T. Ebadzadeh, "Ultra-low temperature fabrication of vanadium carbide reinforced aluminum nano composite through spark plasma sintering," *J. Alloys Compd.*, vol. 753, pp. 433–445, 2018.

[39] D. Sciti, L. Pienti, D. D. Fabbriche, S. Guicciardi, and L. Silvestroni, "Combined effect of SiC chopped fibers and SiC whiskers on the toughening of ZrB_2," *Ceram. Int.*, vol. 40, no. 3, pp. 4819–4826, 2014.

[40] H.-L. Wang *et al.*, "Preparation and characterization of ZrB_2-SiC ultra-high temperature ceramics by microwave sintering," *Front. Mater. Sci. China*, vol. 4, no. 3, pp. 276–280, 2010.

[41] T. Zhu, L. Xu, X. Zhang, W. Han, P. Hu, and L. Weng, "Densification, microstructure and mechanical properties of ZrB_2–SiC_w ceramic composites," *J. Eur. Ceram. Soc.*, vol. 29, no. 13, pp. 2893–2901, 2009.

[42] P. Zhang, P. Hu, X. Zhang, J. Han, and S. Meng, "Processing and characterization of ZrB_2–SiC_w ultra-high temperature ceramics," *J. Alloys Compd.*, vol. 472, no. 1–2, pp. 358–362, 2009.

[43] A. Babapoor, G. Karimi, S. I. Golestaneh, and M. A. Mezjin, "Coaxial electro-spun PEG/PA6 composite fibers: fabrication and characterization," *Appl. Therm. Eng.*, vol. 118, pp. 398–407, 2017.

[44] E. Ghasali, M. Alizadeh, and T. Ebadzadeh, "TiO_2 ceramic particles-reinforced aluminum matrix composite prepared by conventional, microwave, and spark plasma sintering," *J. Compos. Mater.*, p. 002199831775128, 2017.

[45] M. Shokouhimehr, M. Shahedi Asl, and B. Mazinani, "Modulated large-pore mesoporous silica as an efficient base catalyst for the Henry reaction," *Res. Chem. Intermed.*, vol. 44, no. 3, pp. 1617–1626, 2018.

[46] S. Du, L. Xu, X. Zhang, P. Hu, and W. Han, "Effect of sintering temperature and holding time on the microstructure and mechanical properties of ZrB_2–SiC_w composites," *Mater. Chem. Phys.*, vol. 116, no. 1, pp. 76–80, 2009.

[47] X. Zhang, L. Xu, S. Du, J. Han, P. Hu, and W. Han, "Fabrication and mechanical properties of ZrB_2–SiC_w ceramic matrix composite," *Mater. Lett.*, vol. 62, no. 6–7, pp. 1058–1060, 2008.

[48] X. Zhang, L. Xu, W. Han, L. Weng, J. Han, and S. Du, "Microstructure and properties of silicon carbide whisker reinforced zirconium diboride ultra-high temperature ceramics," *Solid State Sci.*, vol. 11, no. 1, pp. 156–161, 2009.

[49] K. Farhadi, A. Sabahi Namini, M. Shahedi Asl, A. Mohammadzadeh, and M. Ghassemi Kakroudi, "Characterization of hot pressed SiC whisker reinforced TiB_2 based composites," *Int. J. Refract. Met. Hard Mater.*, vol. 61, pp. 84–90, 2016.

[50] L. Silvestroni, D. Sciti, C. Melandri, and S. Guicciardi, "Toughened ZrB_2-based ceramics through SiC whisker or SiC chopped fiber additions," *J. Eur. Ceram. Soc.*, vol. 30, no. 11, pp. 2155–2164, 2010.

[51] S. Guicciardi, L. Silvestroni, M. Nygren, and D. Sciti, "Microstructure and toughening mechanisms in spark plasma-sintered ZrB_2 ceramics reinforced by SiC whiskers or SiC-chopped fibers," *J. Am. Ceram. Soc.*, vol. 93, no. 8, pp. 2384–2391, 2010.

[52] D. Chen, L. Xu, X. Zhang, B. Ma, and P. Hu, "Preparation of ZrB_2 based hybrid composites reinforced with SiC whiskers and SiC particles by hot-pressing," *Int. J. Refract. Met. Hard Mater.*, vol. 27, no. 4, pp. 792–795, 2009.

[53] P. Zhang, P. Hu, X. Zhang, J. Han, and S. Meng, "Processing and characterization of ZrB_2–SiC_W ultra-high temperature ceramics," *J. Alloys Compd.*, vol. 472, no. 1–2, pp. 358–362, 2009.

[54] Y. An, X. Xu, and K. Gui, "Effect of SiC whiskers and graphene nanosheets on the mechanical properties of ZrB_2-SiC_w-Graphene ceramic composites," *Ceram. Int.*, vol. 42, no. 12, pp. 14066–14070, 2016.

[55] X. H. Zhang, Z. Wang, P. Hu, W. B. Han, and C. Q. Hong, "Mechanical properties and thermal shock resistance of ZrB_2–SiC ceramic toughened with graphite flake and SiC whiskers," *Scr. Mater.*, vol. 61, no. 8, pp. 809–812, 2009.

[56] W.-M. Guo, Y. You, G.-J. Zhang, S.-H. Wu, and H.-T. Lin, "Improvement of fracture toughness of ZrB_2–SiC composites with carbon interfaces," *J. Eur. Ceram. Soc.*, vol. 35, no. 6, pp. 1985–1989, 2015.

[57] G. R. Anstis, P. Chantikul, B. R. Lawn, and D. B. Marshall, "A critical evaluation of indentation techniques for measuring fracture toughness: I, direct crack measurements," *J. Am. Ceram. Soc.*, vol. 64, no. 9, pp. 533–538, 1981.

[58] M. Shahedi Asl, M. Jaberi Zamharir, Z. Ahmadi, and S. Parvizi, "Effects of nano-graphite content on the characteristics of spark plasma sintered ZrB_2–SiC composites," *Mater. Sci. Eng. A*, vol. 716, pp. 99–106, 2018.

[59] M. Shahedi Asl, "A statistical approach towards processing optimization of ZrB_2–SiC–graphite nanocomposites. Part I: relative density," *Ceram. Int.*, vol. 44, no. 6, pp. 6935–6939, 2018.

[60] S. Parvizi, Z. Ahmadi, M. Jaberi Zamharir, and M. Shahedi Asl, "Synergistic effects of graphite nano-flakes and submicron SiC particles on the characteristics of spark plasma sintered ZrB_2 nanocomposites," *Int. J. Refract. Met. Hard Mater.*, vol. 75, pp. 10–17, 2018.

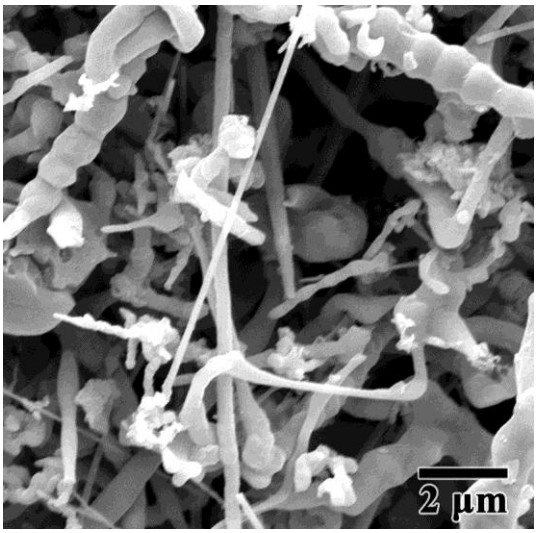

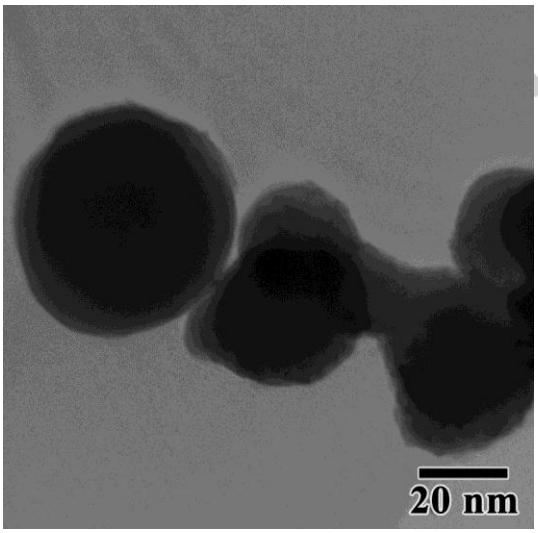

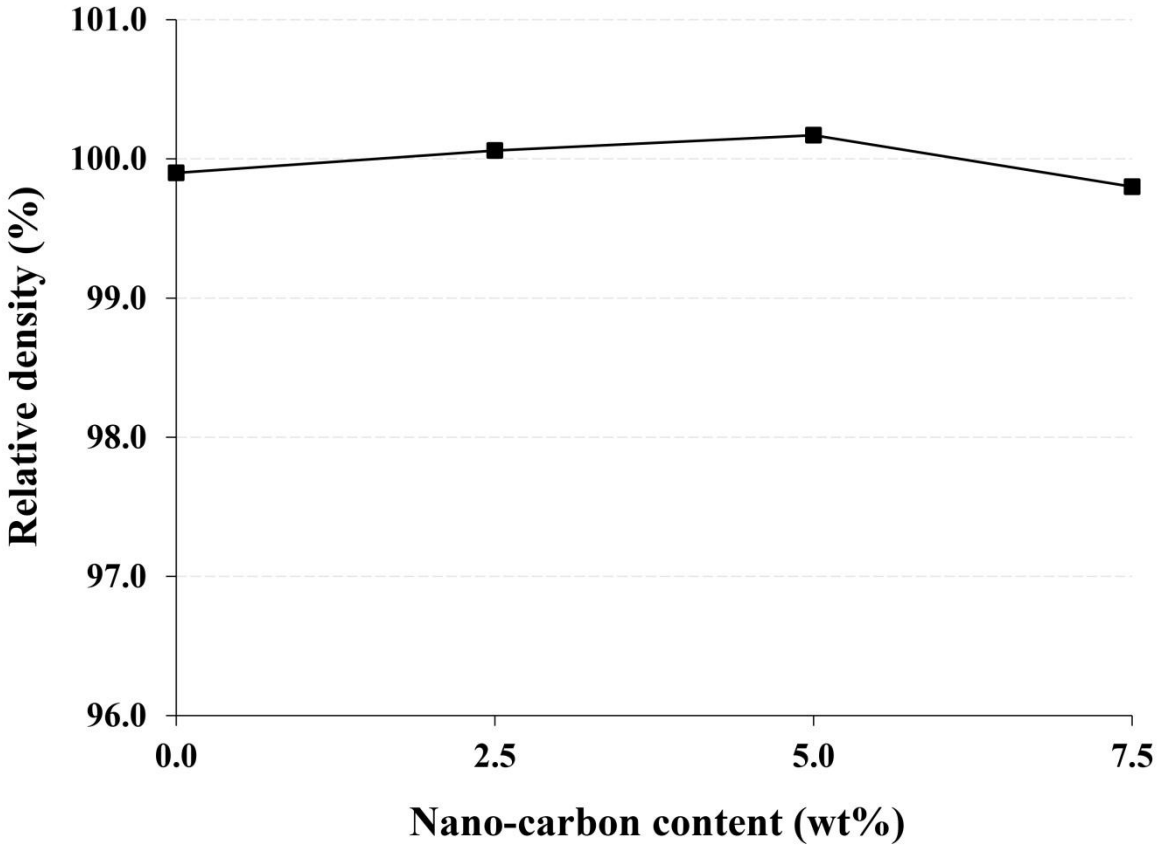

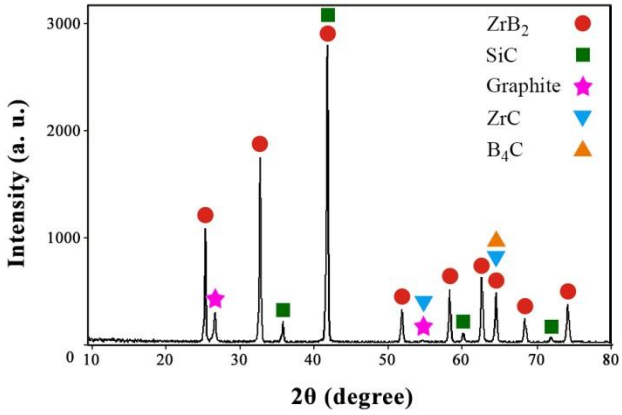

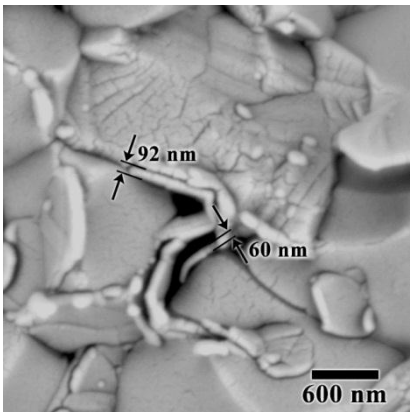

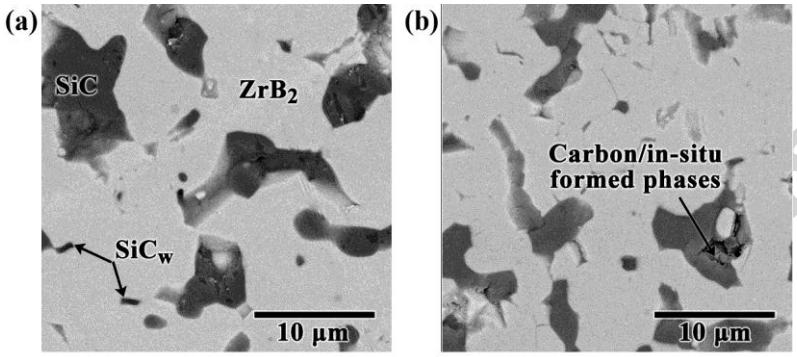

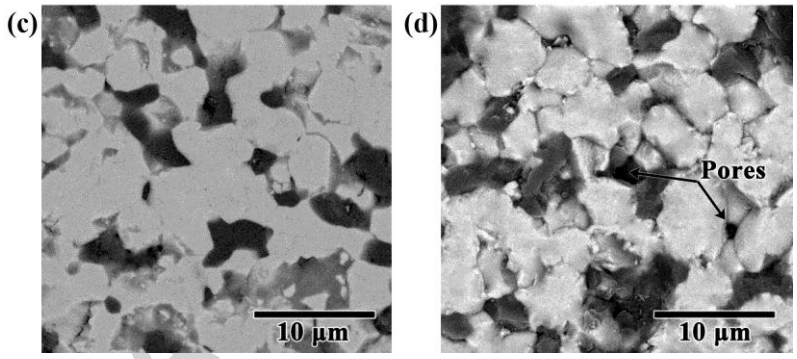

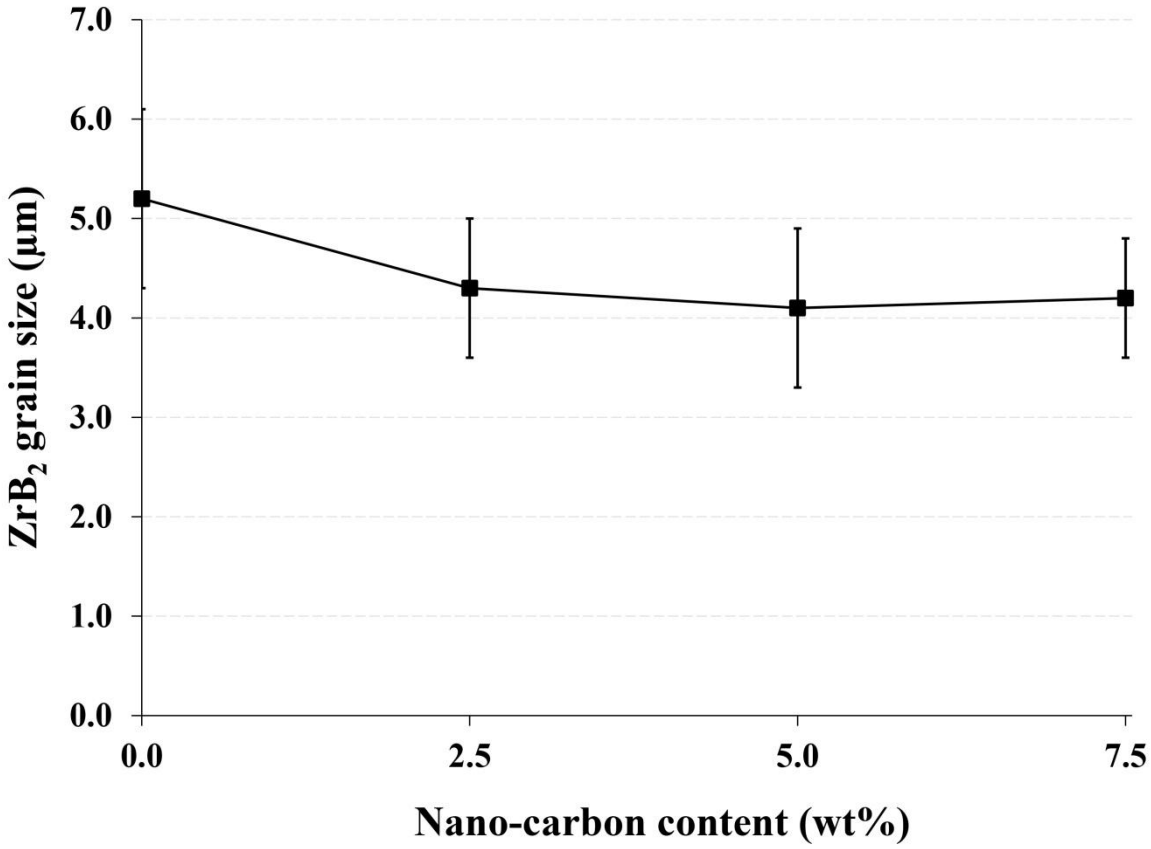

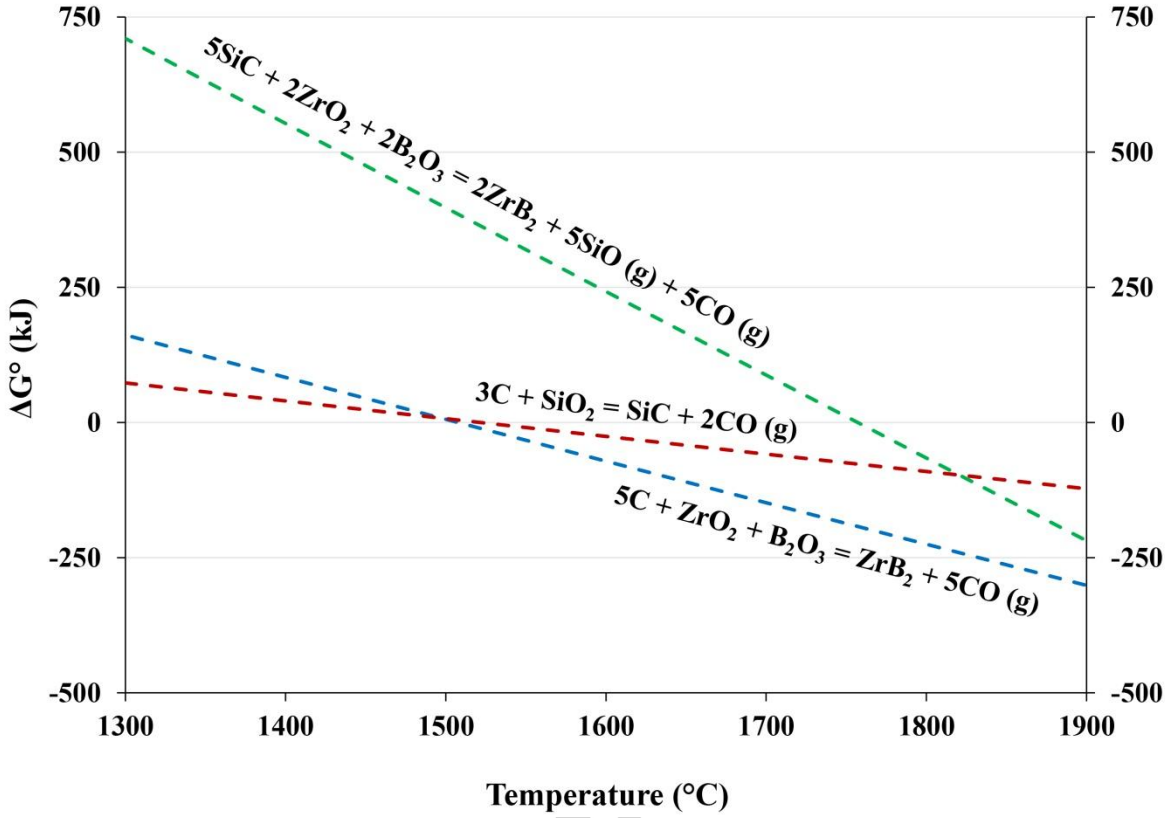
750
500
250
0
-250
-500
1300
1400
1500
1600
1700
1800
1900
ΔG° (kJ)
Temperature (°C)
5SiC + 2ZrO2 + 2B2O3 = 2ZrB2 + 5SiO (g) + 5CO (g)
3C + SiO2 = SiC + 2CO (g)
5C + ZrO2 + B2O3 = ZrB2 + 5CO (g)

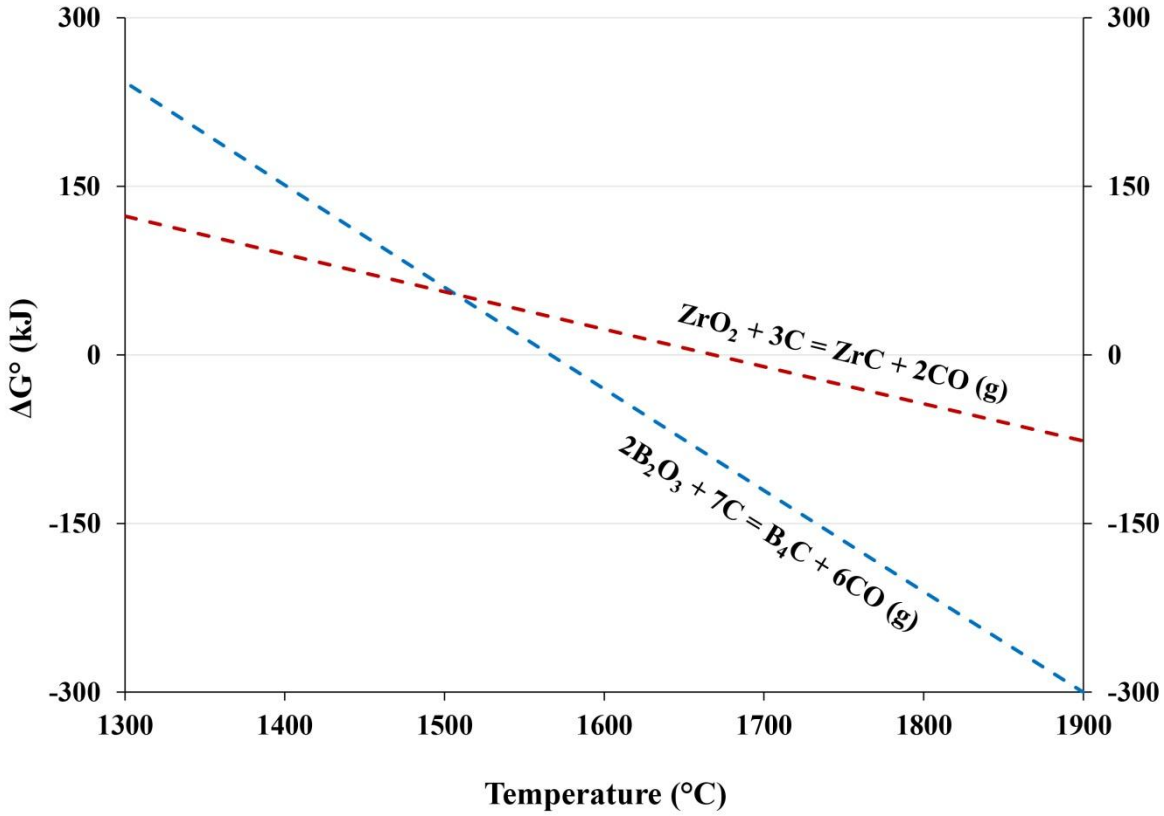
300
150
0
-150
-300
ΔG° (kJ)
1300
1400
1500
1600
1700
1800
1900
Temperature (°C)
ZrO2 + 3C = ZrC + 2CO (g)
2B2O3 + 7C = B4C + 6CO (g)

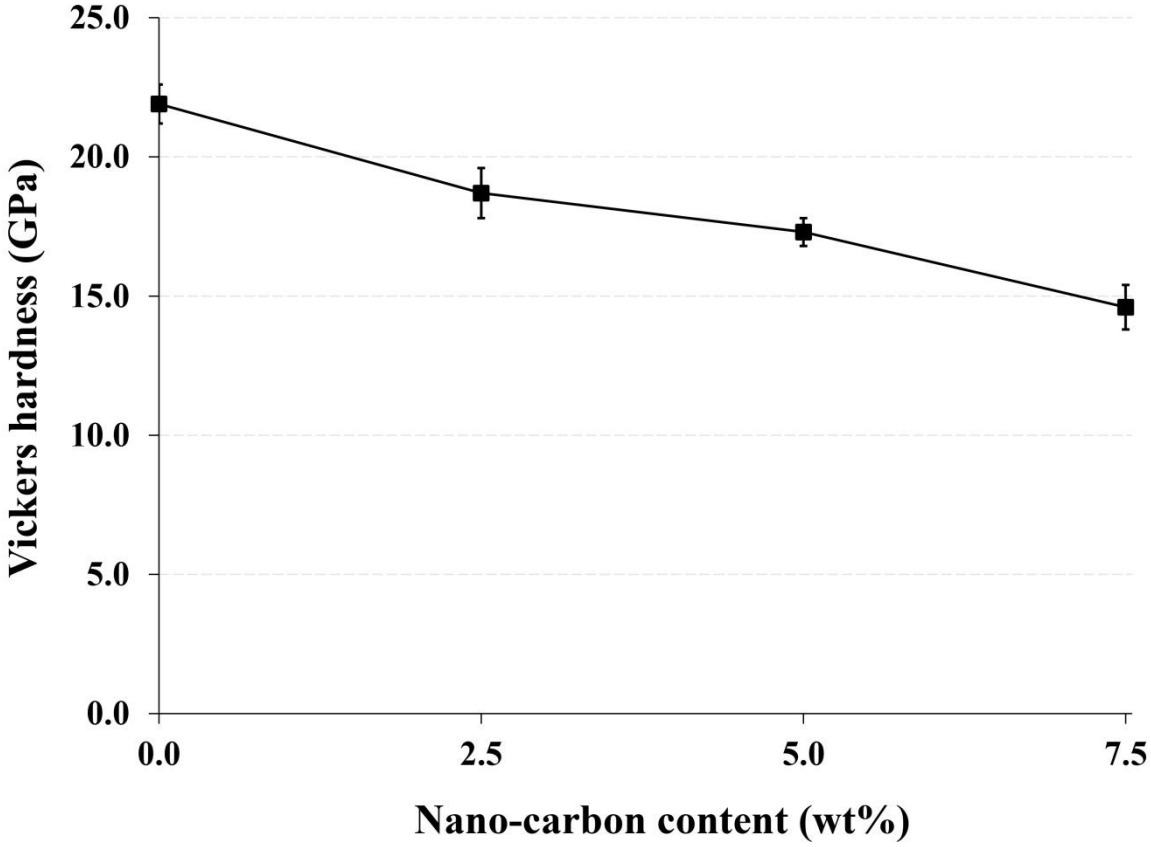

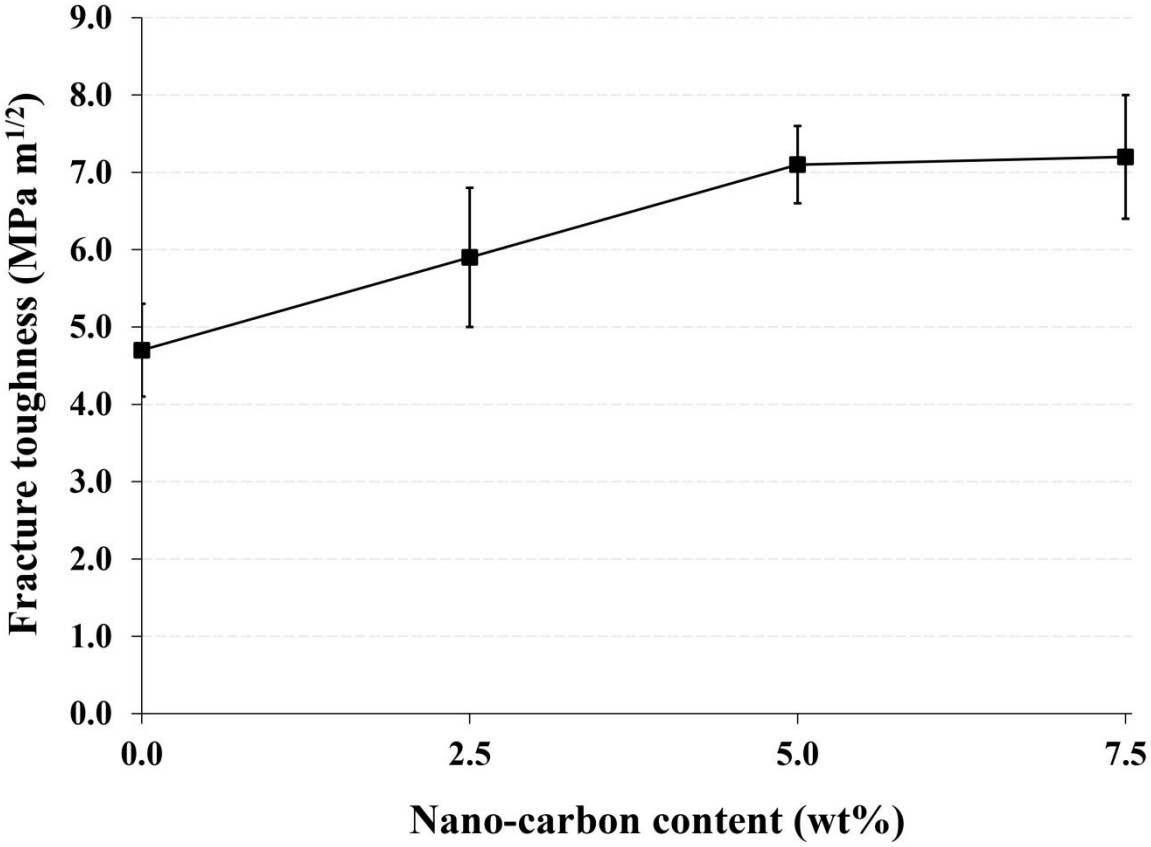
Fracture toughness (MPa m1/2)
9.0
8.0
7.0
6.0
5.0
4.0
3.0
2.0
1.0
0.0
0.0
2.5
5.0
7.5
Nano-carbon content (wt%)

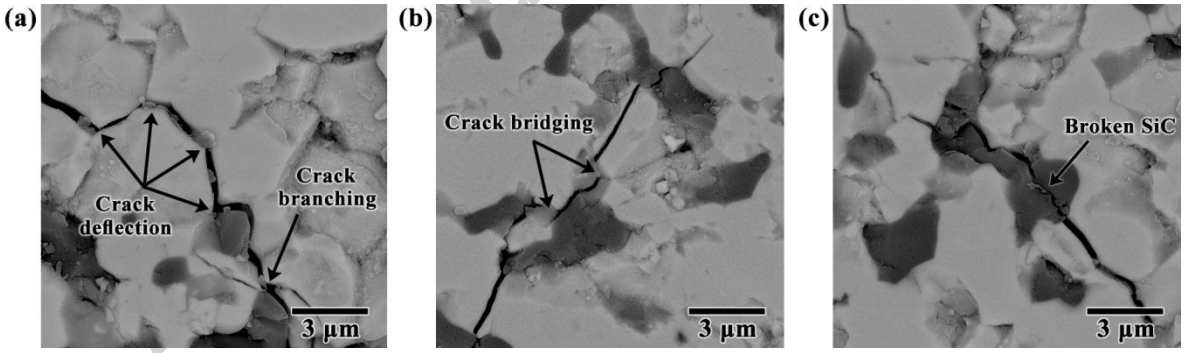
(a)
Crack deflection
Crack branching
3 μm
(b)
Crack bridging
3 μm
(c)
Broken SiC
3 μm